PHYSICAL REVIEW A **73**, 051801(R) (2006)

Controlling the polarization rotation of an optical field via asymmetry in electromagnetically induced transparency

Bo Wang,[1] Shujing Li,[1] Jie Ma,[1] Hai Wang,[1,*] K. C. Peng,[1] and Min Xiao[1,2]
[1]*The State Key Laboratory of Quantum Optics and Quantum Optics Devices, Institute of Opto-Electronics, Shanxi University, Taiyuan 030006, People's Republic of China*
[2]*Department of Physics, University of Arkansas, Fayetteville, Arkansas 72701, USA*
(Received 11 November 2005; revised manuscript received 10 March 2006; published 3 May 2006)

We propose and experimentally demonstrate a mechanism to achieve coherent control of the polarization rotation of an optical field in a multilevel electromagnetically induced transparency (EIT) system in rubidium atoms. By choosing a properly polarized coupling field and transition energy levels, the symmetry of the atomic medium to the propagation of two orthogonal polarization components of a weak linearly polarized probe field can be broken, which leads to a coherently controlled rotation of the probe field polarization. This mechanism of coherently controlled optical polarization rotation makes use of asymmetry in EIT subsystems for the two circular polarization components of the probe beam with a contribution from different transition strengths (due to different Clebsh-Gordan coefficients) in this multilevel atomic system.

DOI: 10.1103/PhysRevA.73.051801 PACS number(s): 42.50.Gy, 33.55.Ad, 42.25.Ja

A linearly polarized light beam will experience a polarization rotation when passing through a chiral medium. The chirality of the medium can be caused by either the intrinsic helicity of the molecules in the medium (called optical activity) or induced by external electrical or magnetic fields. For example, when a magnetic field is applied along the direction of the light beam propagation in an atomic medium, the asymmetry in Zeeman level splittings of the atoms will produce a polarization rotation for the linearly polarized light beam, which is the well-known Faraday effect. Optical fields can also induce chirality in an atomic medium through optical pumping [1], resonant two-photon dispersion [2], magneto-optical effects [3,4], self-induced birefringence [5], etc. In the past few years, several groups had experimentally demonstrated optical birefringence by using a circularly polarized laser beam to change the polarization rotation of a weak linearly polarized probe beam in multilevel ladder-type atomic systems [6–8]. In these experiments, the asymmetry for the two circularly polarized components (σ^+ and σ^-) of the probe beam, therefore the optical birefringence, is generated by the circularly polarized coupling laser beam in the ladder configuration connecting to only one of the two probe circular polarization components. In this situation, strong circular dichroism always exists, which is the major limitation of such experimental systems. Also, control and enhancement of magneto-optical polarization rotation of a laser beam by another coupling laser beam [9] and electromagnetically induced magnetochiral anisotropy in a resonant medium [10] have been proposed, and the latter effect was experimentally demonstrated recently [11].

In this paper, we propose and experimentally demonstrate a system to achieve large optical polarization rotation (up to 45°) of a linearly polarized probe beam controlled by a coupling laser beam under the condition of electromagnetically induced transparency (EIT) in a Λ-type configuration [12,13]. The relevant atomic levels of ^{87}Rb atoms are shown in Fig. 1. We denote Zeeman sublevels of $5S_{1/2}$, $F=1$ as $|a_i\rangle$ ($i=1,2,3$ for $m=-1,0,+1$), of $5S_{1/2}$, $F=2$ as $|b_j\rangle$ ($j=1-5$ for $m=-2,-1,0,+1,+2$), and of $5P_{1/2}$, $F'=2$ as $|c_k\rangle$ ($k=1-5$ for $m=-2,-1,0,+1,+2$), respectively. When both the probe and coupling laser beams are linearly polarized, this system is completely symmetric to the two circular polarization components of the probe beam for realizing EIT as demonstrated in Ref. [13]. We choose the coupling beam (with frequency ω_c) to be a left-circularly polarized (σ^-) beam driving the $|b_{j+1}\rangle$ to $|c_j\rangle$ transitions. The probe beam (with frequency ω_p) is a linearly polarized laser beam consisting of two circularly polarized components σ^- and σ^+, which are near resonant with transitions between levels $|a_i\rangle$ and $|c_k\rangle$. We can clearly see that the left-circularly polarized coupling beam (E_c^-) and the left-circularly polarized probe beam (E_p^-) form three simple Λ-type EIT systems, while E_c^- and the right-circularly polarized probe beam (E_p^+) form only two simple Λ-type EIT systems. This asymmetry in the EIT subsystems for the two circular probe beam components is the key for causing the chirality in this special atomic system. The major advantages of this scheme, compared to the previously demonstrated schemes [6–8], include relative low

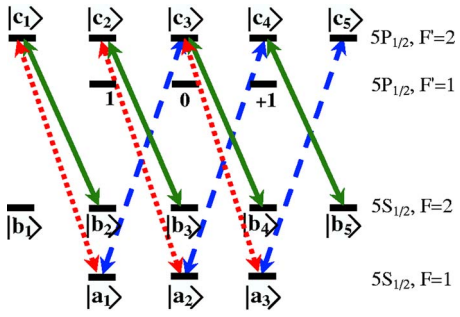

FIG. 1. (Color online) Relevant energy diagram of the D1 line in a ^{87}Rb atom. Solid lines: transitions for the left-circularly polarized coupling beam; dotted lines: transitions for the left-circularly polarized probe beam; dashed lines: transitions for the right-circularly polarized probe beam

*Corresponding author; e-mail address: wanghai@sxu.edu.cn

 ©2006 The American Physical Society

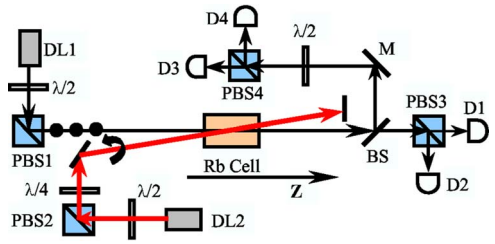

FIG. 2. (Color online) Schematic for the experimental setup. DL1 and DL2: diode lasers; PBS1–PBS4: polarization cube beam splitters; λ/2 and λ/4: half- and quarter-wave plates; D1–D4: photodetectors.

losses for both probe circularly polarized components due to EIT (similar to the recently proposed scheme of using a modified ladder system [14]), high efficiency (a large rotation angle can be achieved with relatively low coupling power), and easy to control (polarization control can be achieved by coupling power, probe frequency detuning, and temperature). This system is very simple and unique (but largely overlooked in this regard), since this scheme only works in certain energy level configurations.

Figure 2 depicts the experimental setup. DL1 (probe beam) and DL2 (coupling beam) are both frequency-stabilized diode lasers with grating feedback. The probe beam is linearly polarized in the *s* direction and the coupling beam is left-circularly polarized by using a polarization beam splitter (PBS2) and a quarter-wave plate. The atomic cell is 5 cm long with magnetic shielding and is temperature stabilized to achieve the desired atomic density. The probe transmission is split into two parts by a 50/50 beam splitter (BS), whose reflectivity is balanced for *s* and *p* linearly polarized laser beams. The reflected beam goes through a half-wave plate whose polarization axis is set at 22.5° from the input probe polarization direction, so it rotates the probe polarization by 45° relative to the input probe beam (when there is no coupling beam). PBS3 splits the two polarization components of the transmitted probe beam from BS into detectors D1 and D2, and PBS4 splits the reflected probe beam from BS into D3 and D4, respectively. The output intensity difference of D3−D4 is proportional to $\sin 2\phi$, where ϕ is the rotated angle of the probe beam in the atomic medium, while the output intensity difference of D1−D2 is proportional to $\cos 2\phi$. Therefore, the rotation angle ϕ can be determined by [3,15]:

$$\phi = \frac{1}{2}\arctan\left[\frac{I_{D3} - I_{D4}}{I_{D1} - I_{D2}}\right], \tag{1}$$

where I_{Di} are the detected intensities of the detectors Di ($i=1-4$), respectively. The main advantage of this detection scheme is to eliminate the effect due to the absorption of the atomic medium in measuring the birefringence of the probe beam, especially since the variation of absorption near the edge of the EIT window is quite large.

The asymmetry in the number of EIT subsystems for the two circularly polarized probe components can easily be checked by adding a magnetic field (~10 G) in the *z* direction of the atomic cell. When the probe beam only had a σ^- component (by using a quarter-wave plate, not shown, in the probe beam before entering the cell), three EIT peaks were observed in the probe transmission (with a σ^- coupling beam) corresponding to the three simple EIT subsystems. As the magnetic field was turned off, a degenerate EIT peak, as shown in Fig. 3(a), was recorded. However, if the probe beam only had a σ^+ component (with the σ^- coupling beam and a magnetic field of ~10 G), only two EIT peaks were seen. Again, by turning off the magnetic field, a degenerate EIT peak in this configuration was measured, as shown in Fig. 3(b). It is clear from Figs. 3(a) and 3(b) that the EIT widths and heights for these two circularly polarized probe components are quite different due to the asymmetry in the number of degenerate EIT subsystems and a minor contribution from the differences in the transition strengths (due to the differences between the Clebsch-Gordan coefficients). This indicates that a linearly polarized probe beam will experience birefringence, especially at the edges of the EIT windows. The dispersion corresponding to the difference of these two EIT curves [Figs. 3(a) and 3(b)] represents the relative phase shifts, and therefore the rotation angles, of the linearly polarized probe beam. Figure 3(c) is the detected optical power by detector D1 as a function of probe frequency detuning. Without the coupling beam, the *s*-polarized probe beam will be totally reflected by PBS3 and no light will be detected by D1. As the left-circularly polarized coupling beam (E_c^-) is turned on, part of the probe beam is rotated to pass PBS3 caused by light-induced chirality and detected by D1. In this system, the maximum polarization

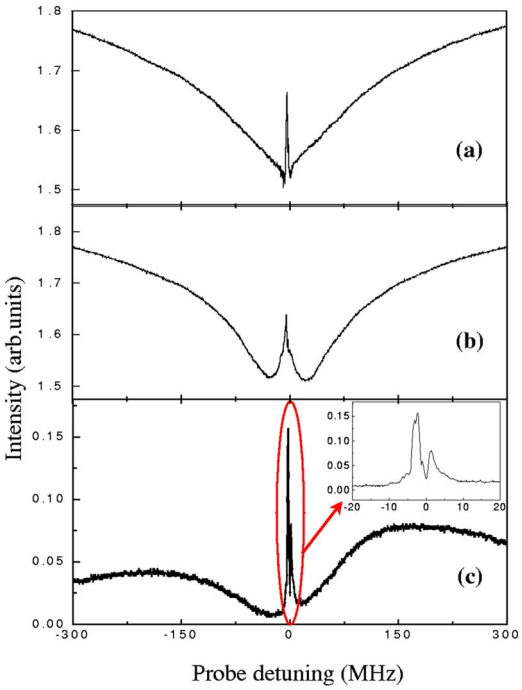

FIG. 3. (Color online) EIT curves for left-circularly polarized coupling beam with (a) left-circularly polarized probe beam and (b) right-circularly polarized probe beam, respectively. Probe beam power is 75 μW. (c) The detected intensity of rotated linearly polarized probe beam (power of 150 μW) detected by D1, power of the left-circularly polarized coupling beam is 8 mW.

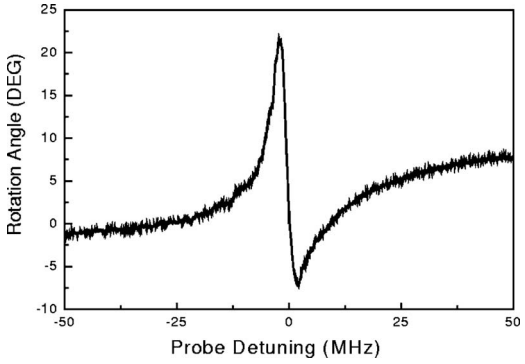

FIG. 4. Experimental measured degree of polarization rotation as a function of probe detuning. Probe beam power is 150 μW, coupling power is 15 mW, and the temperature of the Rb vapor cell is 55 °C.

rotation occurs at two dispersion peaks [see the inset of Fig. 3(c)] coming out of the difference in the EIT windows for the two circularly polarized probe components. The left (right) peak corresponds to a positive (negative) dispersion [i.e., $\mathrm{Re}(\chi_p^+ - \chi_p^-) \geqslant 0$ ($\leqslant 0$), where χ_p^+ and χ_p^- are the susceptibilities for the right- and left-circularly polarized probe components, respectively), which gives a counterclockwise (clockwise) polarization rotation. With the signal data detected from D1, D2, D3, and D4, we further obtained the degree-of-polarization rotation by Eq. (1) as a function of probe detuning, as shown in Fig. 4. This shows that if the probe frequency is changed from one of the dispersion peaks to the other peak, the total change in the polarization rotation angle will be larger for the probe beam, which can have interesting applications.

The polarization rotation angle can be calculated by considering all relevant atomic energy levels as depicted in Fig. 1. In the interaction picture and under the dipole and rotating-wave approximations, the Hamiltonian can be described by

$$\begin{aligned}\hat{H}_{\mathrm{int}} = &-\hbar\sum_{i=1}^{5}\Delta\omega_p|c_i\rangle\langle c_i| - \hbar\sum_{i=1}^{4}\Delta\omega_{ci}|b_{i+1}\rangle\langle b_{i+1}| \\ &-\frac{\hbar}{2}\left[\sum_{i=1}^{3}\Omega_{pi}^-|c_i\rangle\langle a_i| + \sum_{i=1}^{3}\Omega_{pi}^+|c_{i+2}\rangle\langle a_i| + \mathrm{c.c.}\right] \\ &-\frac{\hbar}{2}\left[\sum_{i=1}^{4}\Omega_{ci}^-|c_i\rangle\langle b_{i+1}| + \mathrm{c.c.}\right],\end{aligned} \tag{2}$$

where $\Delta\omega_p = \omega_p - \omega_{ac}$, $\Delta\omega_{ci} = \Delta\omega_p - (\omega_c - \omega_{ci,bi+1})$. $\omega_{ci,bi+1}$ is the transition frequency from c_i to b_{i+1}. $\Omega_{pi}^- = -\mu_{ci,ai}E_p^-/\hbar$, $\Omega_{pi}^+ = -\mu_{ci+2,ai}E_p^+/\hbar$, and $\Omega_{ci}^- = -\mu_{ci,bi+1}E_c^-/\hbar$ are the Rabi frequencies of the probe and coupling beams for the specific transitions with corresponding transition dipole moments $\mu_{i,j}$, respectively. Differences in transition probabilities (Clebsch-Gordan coefficients of the transitions) between different energy levels [16] are taken into account in determining these Rabi frequencies for different transitions. Since the strong coupling laser beam also interacts with the levels in $5P_{1/2}$, $F'=1$ ($m=-1,0,+1$) with a frequency detuning of $\Delta = 2\pi \times 816$ MHz, it induces different ac Stark shifts $\hbar\delta_{b3} = \hbar(|\Omega_{C,b3}^-|^2/4\Delta)$, $\hbar\delta_{b4} = \hbar(|\Omega_{C,b4}^-|^2/4\Delta)$, and $\hbar\delta_{b5} = \hbar(|\Omega_{C,b5}^-|^2/4\Delta)$ for the energy levels $|b_3\rangle$, $|b_4\rangle$, and $|b_5\rangle$ [17] (where $\Omega_{C,bi}^- = \mu_{m,bi}E_c^-/\hbar$ are the Rabi frequencies of the coupling beam for the transitions from levels b_i ($i=3,4,5$) to the Zeeman sublevels $m=-1,0,+1$ of $5P_{1/2}$, $F'=1$), which affect frequency detunings of the coupling beam with transitions from $|b_{i+1}\rangle$ to $|c_i\rangle$. The susceptibilities for the right- and left-circularly polarized probe components can be represented as

$$\begin{aligned}\chi_p^- &= -\frac{N}{\hbar\varepsilon_0}\left[\frac{|\mu_{c_1,a_1}|^2}{\Omega_{p1}^-}\rho_{a_1,c_1} + \frac{|\mu_{c_2,a_2}|^2}{\Omega_{p2}^-}\rho_{a_2,c_2} + \frac{|\mu_{c_3,a_3}|^2}{\Omega_{p3}^-}\rho_{a_3,c_3}\right], \\ \chi_p^+ &= -\frac{N}{\hbar\varepsilon_0}\left[\frac{|\mu_{c_3,a_1}|^2}{\Omega_{p1}^+}\rho_{a_1,c_3} + \frac{|\mu_{c_4,a_2}|^2}{\Omega_{p2}^+}\rho_{a_2,c_4} + \frac{|\mu_{c_5,a_3}|^2}{\Omega_{p3}^+}\rho_{a_3,c_5}\right].\end{aligned} \tag{3}$$

The density-matrix elements $\rho_{ai,ck}$ can be calculated from the master equation

$$\frac{\partial\hat{\rho}}{\partial t} = -\frac{i}{\hbar}(\hat{H}_{\mathrm{int}},\hat{\rho}) + \left(\frac{\partial\hat{\rho}}{\partial t}\right)_{inc}, \tag{4}$$

where the first term is the contribution of coherent interaction and the second term results from the contribution of the dampings. N is the atomic density. We can obtain the approximate expressions for the above density-matrix elements $\rho_{ai,ck}$ under the steady-state and weak probe conditions. The results show that coherent matrix elements ρ_{a_1,c_1}, ρ_{a_2,c_2}, ρ_{a_3,c_3}, ρ_{a_1,c_3}, ρ_{a_2,c_4} can be enhanced by EIT subsystems formed by three-level systems b_2-c_1-a_1, b_3-c_2-a_2, b_4-c_3-a_3, b_4-c_3-a_1, b_5-c_4-a_2, respectively, while ρ_{a_3,c_5} is not enhanced. The polarization rotation angle of the probe beam is then given by

$$\phi = \frac{\pi}{2\lambda}\,\mathrm{Re}(\chi_p^+ - \chi_p^-)d, \tag{5}$$

where d is the length of the atomic cell. The Doppler effect of atoms in a vapor cell is included by integrating over an atomic velocity distribution [13]. Equation (5) shows that ϕ is dependent on the difference between χ_p^+ and χ_p^-.

The calculated and experimentally measured rotation angles for the two dispersion peaks (at different probe frequency detunings) as a function of the coupling beam power are plotted in Fig. 5. Although the rotation angles of both dispersion peaks increase with the coupling beam power, they have a different dependence on the coupling beam power. Such asymmetry is partly caused by different Stark shifts involving the additional energy levels of $5P_{1/2}$, $F'=1$, which give different coupling beam frequency detunings for different transitions and make the centers of transmission and dispersion profiles of the Λ-type EIT subsystems shift by different values. Similar to the phenomenon of linear magneto-optical rotation [3], the asymmetric ac Stark shifts also cause optical birefringence for the probe beam. Experimentally, the rotation angles are measured by using the two pairs of detectors as described in Eq. (1). The probe power of

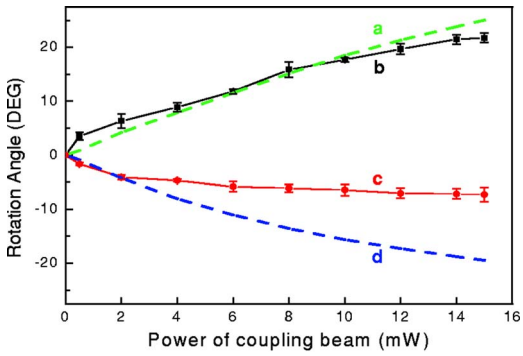

FIG. 5. (Color online) Degree of polarization rotation as a function of the coupling beam power. (b) and (c) are experimental results for the left and right dispersion peaks, respectively; (a) and (d) are theoretical results for the left and right dispersion peaks, respectively, with parameters $\gamma_{ab}=2\pi\times 1.1$ MHz, $\gamma_{ac}=2\pi\times 3.5$ MHz, and atomic density of $N=1.62\times 10^{11}/\mathrm{cm}^3$.

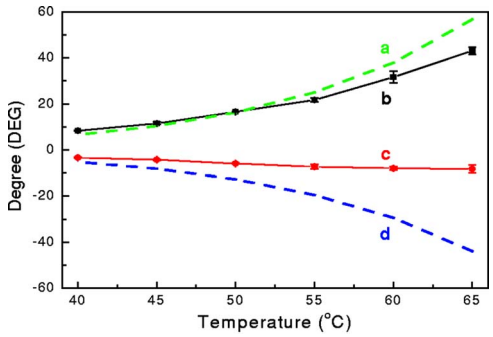

FIG. 6. (Color online) Degree of polarization rotation as a function of the temperature of the Rb vapor cell. (b) and (c) are experimental results for the left and right dispersion peaks, respectively, with a coupling power 15 mW; (a) and (d) are theoretical results with parameters $\gamma_{ab}=2\pi\times 1.1$ MHz, $\gamma_{ac}=2\pi\times 3.5$ MHz, $\Omega_c=2\pi\times 100$ MHz.

150 μW (corresponding to the Rabi frequency of $\Omega_p=2\pi\times 10$ MHz) is used. The ground-state population distributions can be calculated from Eq. (4) (for example, we get $\rho_{a_1,a_1}=0.229$, $\rho_{a_2,a_2}=0.235$, $\rho_{a_3,a_3}=0.065$ when $\Omega_c=2\pi\times 100$ MHz, $\Omega_p=2\pi\times 10$ MHz, $\gamma_{ac}=2\pi\times 3.5$ MHz, and $\gamma_{ab}=2\pi\times 1.1$ MHz). The temperature of the vapor cell was set at 55 °C during the measurements corresponding to an atomic density of $N=1.62\times 10^{11}/\mathrm{cm}^3$. The theoretically calculated degree of polarization rotation matches very well with the measured data of the left dispersion peak, but is off substantially with the data for the right peak. We are currently investigating possible explanations for such a discrepancy in Fig. 5.

Since this optical chirality effect depends sensitively on the widths and heights of the EIT windows for the two circular polarization components of the probe beam, it will be very sensitive to the temperature change of the atomic medium. Figure 6 plots the experimentally measured and theoretically calculated polarization rotation angles of the probe beam for the two dispersion peaks as a function of the temperature. The coupling power used in this figure is about 15 mW (corresponding to the Rabi frequency of $\Omega_c=2\pi\times 100$ MHz). It is clear that the optical polarization rotation of one laser (probe) beam can be well controlled by another (coupling) laser beam. A quite large polarization rotation angle (~45°) can be realized by using a relatively low coupling beam power, which gives a significant advantage over previously demonstrated schemes. Actually, by changing the probe frequency from one of the dispersion peaks to another will give an even larger polarization rotation angle for the probe beam. Due to the EIT nature of the current scheme, absorption loss of the probe beam is relatively small even at high temperatures, which is an important advantage.

In summary, we had demonstrated a new scheme to coherently control the polarization rotation of a linearly polarized probe beam by a circularly polarized coupling beam in a unique multilevel Λ-type atomic medium. The large rotation angle with a relatively low controlling optical power makes it potentially very useful as polarization elements (half-wave plate) in atomic assembles. Another interesting feature of this scheme is the sensitive dependence of the rotation angle on the probe beam frequency detuning, which can be used to construct a controlled optical switch (or logic gate) with small frequency detuning.

We acknowledge funding support from the NSFC (Contract No. 60325414, Contract No. 60578059, Contract No. RGC60518001), NSF of Shanxi Province (Contract No. 20031007), and Shanxi Returned Scholar Funds. M.X. also acknowledges funding support from NSF (Contract No. PHY-0354657) in the United States.

[1] C. Cohen-Tannoudji and J. Dupont-Roc, Phys. Rev. A **5**, 968 (1972).
[2] P. F. Liao and G. C. Bjorklund, Phys. Rev. Lett. **36**, 584 (1976).
[3] D. Budker *et al.*, Rev. Mod. Phys. **74**, 1153 (2002); and references therein.
[4] I. Novikova *et al.*, Opt. Lett. **26**, 1016 (2001).
[5] S. M. Rochester *et al.*, Phys. Rev. A **63**, 043814 (2001).
[6] F. S. Pavone *et al.*, Opt. Lett. **22**, 736 (1997).
[7] S. Wielandy and A. L. Gaeta, Phys. Rev. Lett. **81**, 3359 (1998).
[8] T. H. Yoon *et al.*, Phys. Rev. A **70**, 061803(R) (2004).
[9] A. K. Patnaik and G. S. Agarwal, Opt. Commun. **179**, 97 (2000).
[10] G. S. Agarwal and S. Dasgupta, Phys. Rev. A **67**, 023814 (2003).
[11] V. A. Sautenkov *et al.*, Phys. Rev. Lett. **94**, 233601 (2005).
[12] S. E. Harris, Phys. Today **50**, 36 (1997).
[13] Y. Q. Li and Min Xiao, Phys. Rev. A **51**, R2703 (1995).
[14] D. Cho *et al.*, Phys. Rev. A **72**, 023821 (2005).
[15] C. P. Pearman *et al.*, J. Phys. B **35**, 5141 (2002).
[16] For details in transition probabilities of the D1 line in ^{87}Rb, see http://steck.us/alkalidata.
[17] M. Weidemuller and C. Zimmermann, *Interactions in Ultracold Gases* (Wiley-VCH, Weinheim, 2003).